AIAA JOURNAL
Vol. 35, No. 10, October 1997

# Wavelet Analysis of Wall-Pressure Fluctuations in a Supersonic Blunt-Fin Flow

Jonathan Poggie*
*U.S. Air Force Research Laboratory, Wright–Patterson Air Force Base, Ohio 45433-7913*
and
Alexander J. Smits†
*Princeton University, Princeton, New Jersey 08544-5263*

**Measurements of wall-pressure fluctuations in a Mach 3 flow over a blunt fin were analyzed with the continuous wavelet transform. This technique offers a fresh approach to the problem of inferring flow structure from the wall-pressure signal. The time scales associated with large-scale structures in the flow turbulence and with shock crossing events are identified as distinct local maxima in the distribution of energy over the wavelet scales. By using the extrema in the wavelet spectrum as a reference, the signal can be filtered in the space of wavelet scales to separate the contribution to the pressure fluctuations of flow turbulence and separation shock motion.**

## Nomenclature

| | |
|---|---|
| $a$ | = wavelet scale |
| $b$ | = wavelet translation parameter |
| $C$ | = wavelet reconstruction parameter |
| $D$ | = fin diameter |
| $d$ | = transducer diameter |
| $E$ | = energy |
| $f$ | = frequency |
| $g$ | = wavelet function |
| $m$ | = an integer |
| $p$ | = pressure |
| $R$ | = cross correlation |
| $Re$ | = Reynolds number |
| $S$ | = wavelet transform |
| $s$ | = signal |
| $T$ | = temperature |
| $t$ | = time |
| $U$ | = streamwise component of mean velocity |
| $(x, y, z)$ | = streamwise, wall-normal, and spanwise coordinates |
| $\delta$ | = boundary-layer thickness |
| $\theta$ | = boundary-layer-momentum thickness |
| $\psi$ | = dilated wavelet function |

*Subscripts*

| | |
|---|---|
| $B$ | = boundary layer |
| $e$ | = boundary-layer edge |
| $S$ | = shock wave |
| $t$ | = total |
| $w$ | = wall |
| 0 | = stagnation condition or initial condition |

*Superscripts*

| | |
|---|---|
| $\hat{}$ | = Fourier transform |
| $+$ | = inner scaling for turbulent boundary layer |
| $*$ | = complex conjugate |

Received Aug. 1, 1996; revision received June 14, 1997; accepted for publication June 23, 1997. This paper is declared a work of the U.S. Government and is not subject to copyright protection in the United States.

*Research Aerospace Engineer, Aerodynamic Components Research Branch, Aeromechanics Division, Wright Laboratory, 2645 Fifth Street, Suite 7. Member AIAA.

†Professor, Department of Mechanical and Aerospace Engineering, P.O. Box CN5263. Associate Fellow AIAA.

## Introduction

INTENSE shock oscillation appears to be a universal feature of the interaction of a shock wave and a separated turbulent boundary layer. Although the physical mechanisms governing this shock motion are not well understood, experiments have begun to uncover some of the general features of this phenomenon by resolving the evolution of the flow over time. In particular, the motion of the shock has been tracked directly through flow visualization and indirectly through threshold-based signal analysis of wall-pressure fluctuations.

Shock oscillation appears to occur on two scales: one because of perturbation of the separation zone by turbulence in the boundary layer and the other because of a relatively larger-scale expansion and contraction of the separation bubble, analogous to the cyclic vortex shedding seen in low-speed juncture flows.[1,2] The smaller-scale motion of the separation bubble has a characteristic frequency comparable to that of the boundary-layer structures,[3,4] which in flow visualization experiments[5,6] appear to distort the shock system as they convect downstream. In contrast, the large-scale motion of the separation bubble has a characteristic frequency much lower than that of the organized structures in the upstream boundary layer and tends to be preceded by fluctuations inside the separation bubble.[3,7–9] Separation bubble motion on these two scales has also been observed in incompressible, separated flows[10] and may occur independently in different compressible flows.[6,11]

This study focused on the blunt-fin geometry (Fig. 1a), a configuration that mimics the interaction that can occur on the sidewalls of engine inlets and at the juncture of a wing and fuselage. A horseshoe vortex system and its associated lambda shock system are the dominant features of the three-dimensional, separated flow near such a juncture. Local maxima in the mean and standard deviation of the measured wall pressure and heat flux[12–14] indicate the presence of horseshoe vortices. The vortices are observed directly in numerical simulations as spiraling streamline patterns (foci) near the root of the fin.[15,16] Experimental work[12,13,17–19] has shown that the size of the separated zone scales on the diameter of the rounded leading edge of the fin, with a relatively weak effect of variations in Mach number, Reynolds number, and boundary-layer thickness; numerical simulations[15] have reproduced the weak effect of boundary-layer thickness.

Because of the scaling on the fin diameter, the blunt fin can be considered to produce a dimensional interaction in that the diameter determines the length scale of the interaction. Generally, the scale of the interaction flowfield depends largely on $D$ and only weakly on $\delta_0$. For small values of $D/\delta_0$, the vortex/shock system is contained inside the boundary layer, but as this ratio increases the vortex/shock structure extends outside the layer. For large values of $D/\delta_0$, the interaction becomes independent of $\delta_0$.

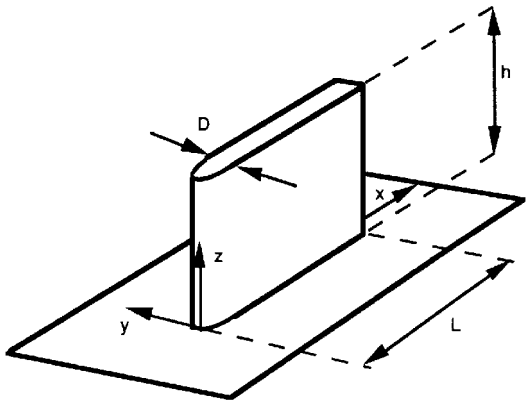


**a) Model geometry and coordinate system**

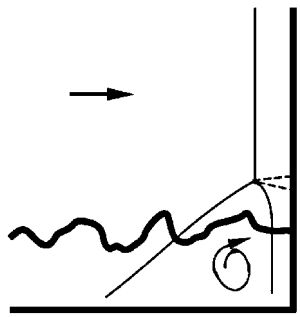

**b) Principal flow features in the plane of the fin centerline**

**Fig. 1 Blunt-fin flow.**

We have restricted our attention in this work to the flow in the plane of symmetry of the fin (Fig. 1b). The structure of the flow in this plane has been examined by schlieren photography[20] and Rayleigh scattering,[21] revealing a lambda-shaped shock system. In the images produced by these methods, a detached normal shock (the bow shock) is visible in the region away from the wall. Typically, two oblique shocks are visible closer to the wall, intersecting the bow shock in a triple point. The upstream oblique shock is called the separation shock, because it encloses the region of recirculating flow associated with the primary horseshoe vortex. (The flow downstream of the instantaneous position of this shock is separated.[22]) The shear layer emanating from the triple point of the shock system impinges onto the nose of the fin, typically creating a zone of high pressure and intense heat flux.[20,23]

Although the bow shock does not move significantly, the separation shock is highly unsteady, and multiple separation shocks are sometimes present.[21] The separation shock moves randomly between the upstream influence line and the mean separation line, causing intense, intermittent, fluctuations in wall pressure.[24] The characteristic frequency of the pressure fluctuations appears to scale on the streamwise extent of the region of shock oscillation[25] and thus approximately on the fin diameter.

This study was designed to determine the length and time scales of the boundary-layer turbulence and the separation vortex system and to study the physical processes that occur at the two scales. To this end, wall-pressure fluctuation measurements made previously[26] in a Mach 3 blunt-fin flow were analyzed by the continuous wavelet transform. (Some preliminary results of this project have been reported elsewhere.[27]) The wavelet transform offers a means of identifying the shock motion in the wall-pressure signal, which is potentially simpler than standard techniques based on thresholds of the signal level.

## Experimental Procedure

The experiments were carried out by Evans et al.[26] in the second test section of the Princeton University $203 \times 203$ mm high Reynolds number blowdown wind tunnel. This facility can operate with stagnation pressures ranging from about 400 to over 1400 kPa and at Mach numbers from 2 to 4. For the data presented here, the stagnation pressure and freestream Mach number were 690 kPa ($\pm 1\%$) and $2.87 \pm 0.01$, respectively. In a typical run, the stagnation temperature was initially 290 K and dropped by about 8% over 2 min. The tests were made under near adiabatic wall conditions ($T_w/T_0 = 1.04$).

The incoming boundary layer has been surveyed extensively by Settles[28] and by Spina and Smits[29] and has been found to be a two-dimensional, fully turbulent, equilibrium boundary layer. In the vicinity of the current test station, the momentum thickness Reynolds number was about $Re_\theta = 78 \times 10^3$, with $\delta = 28$ mm and $\theta = 1.2$ mm. The nominal freestream velocity was taken to be $U_e = 565$ m/s.

The test model geometry and coordinate system are shown in Fig. 1a. The fin is mounted perpendicular to the wind-tunnel floor and is 127 mm long and 122 mm high; the leading edge is a semicircular cylinder with a diameter of 19 mm. The fin is not swept and is at a zero angle of attack. Previous research has shown that the fin can be considered semi-infinite in that further increases in the height of the fin do not affect the flow near the wall.[18]

Static pressure measurements were made on the wall upstream of the fin with six miniature differential pressure transducers manufactured by Kulite Semiconductor Products (model XCQ-72-062-25D). The transducers were mounted in a straight line on a circular plug in the floor of the wind tunnel, and a sting mount allowed the fin to be positioned at different streamwise locations relative to the transducers. The spacing between the transducers was 5.1 mm, and they were mounted on the centerline of the wind tunnel aligned with the fin.

The data were taken with the fin positioned in three locations relative to the plug, covering a range of stations between about 0.5 and 4 fin diameters upstream of the fin.

The transducers were calibrated statically at the operating temperature. Previous studies, and checks made before and after wind-tunnel runs, have shown that the calibration is consistently linear and repeatable.

The signals from the transducers were amplified and then bandpass-filtered with Ithaco four-pole Butterworth filters (rolloff rate, 80 dB/decade). The analog data were then sampled digitally with 10-bit resolution by using a computer-automated measurement and control (CAMAC) system from LeCroy Research Systems, Inc. Three sampling rates were used: 50 kHz, 250 kHz, and 1 MHz. In all three cases, the high-pass filter was set to 10 Hz. The low-pass filter was set to 25 kHz for the 50-kHz sampling rate and was set to 100 kHz otherwise. Data were obtained simultaneously for the six channels in files of four records, each containing 16,384 contiguous points per record.

Previous experimental work suggests that the transducers have an acceptable frequency response up to about 80 kHz, high enough to resolve the large-scale organized structures in the incoming turbulent boundary layer at $U_e/\delta \approx 20$ kHz.

There are no well-established transducer size criteria for fluctuating wall-pressure measurements in turbulent supersonic flow. Dolling and Dussauge[30] give some rules of thumb. Here we note that the diameter $d$ of the transducer sensing element is 0.71 mm, which is substantially smaller than the $\delta$-scale coherent structures present in the incoming boundary-layer flow ($d/\delta \approx 0.03$) but much larger than the smallest-length scales in the flow ($d^+ \approx 300$).

The small-scale, high-frequency component of the wall-pressure signal associated with fine-scale flow turbulence is not resolved by the current pressure measurements and, with the absence of more sensitive transducer technology to make measurements for comparison, the effect of the omitted scales on the results is difficult to quantify. Nevertheless, the spatial and temporal resolution of the pressure transducers was adequate to resolve the pressure fluctuations associated with the shock motion and large-scale turbulence structures that were the focus of this study.

## Method of Analysis

Here we briefly outline the one-dimensional continuous wavelet transform. Application of the continuous wavelet transform to signal analysis is discussed in detail by Vetterli and Kovačević,[31] and Farge[32] gives a comprehensive review of application of the wavelet transform to the study of turbulence.

The continuous wavelet transform is a linear integral transform that associates a function $S(a, b)$ with a signal $s(t)$ according to the definition

$$S(a, b) = \int_{-\infty}^{\infty} \psi^*_{a,b}(t) s(t)\, \mathrm{d}t \tag{1}$$

where

$$\psi_{a,b}(t) = (1/\sqrt{a}) g[(t - b)/a] \tag{2}$$

is the mother wavelet $g(t)$ stretched by the scale $a$ and translated by $b$. The weighting function $1/\sqrt{a}$ is chosen so that the energy (integral of the squared magnitude) in the dilated wavelet function is the same for all scales.

Equation (1) represents the inner product of the signal with the translated and dilated wavelet function and is similar in form to a correlation or convolution integral. Therefore, the wavelet transform has a large magnitude when the dilated wavelet and the signal are similar in shape.

It is possible to reconstruct the original signal from the wavelet transform through the following formula:

$$s(t) = \frac{1}{C_\psi} \int_{0^+}^{\infty} \int_{-\infty}^{\infty} \frac{1}{a^2} S(a, b) \psi_{a,b}(t)\, \mathrm{d}b\, \mathrm{d}a \tag{3}$$

where

$$C_\psi = \int_{0^+}^{\infty} \frac{|\hat{g}(f)|^2}{f}\, \mathrm{d}f \tag{4}$$

is the reconstruction parameter and $\hat{g}(f)$ is the Fourier transform of the mother wavelet. We have assumed here that $|\hat{g}(f)|^2$ is an even function and require that $C_\psi$ has a value between zero and infinity. These restrictions are satisfied by the real functions with zero mean and finite energy that we have selected for use in this study.

A wavelet energy spectrum can be defined that describes distribution of the energy in the signal over the wavelet scales. This form allows the energy in each wavelet scale to be interpreted in a manner analogous to the Fourier energy spectrum. The total energy in the signal is defined as

$$E_t = \int_{-\infty}^{\infty} |s(t)|^2\, \mathrm{d}t = \int_{0^+}^{\infty} E(a)\, \mathrm{d}a \tag{5}$$

where

$$E(a) = \frac{1}{a^2 C_\psi} \int_{-\infty}^{\infty} |S(a, b)|^2\, \mathrm{d}b \tag{6}$$

is the distribution of energy over the wavelet scales.

Two simple wavelet functions were used in the following analyses. The Mexican hat wavelet is the negative of the second derivative of a Gaussian function and is useful for detecting peaks in a signal (Figs. 2a and 2b). The Mexican hat function has the following form:

$$g(t) = (1 - t^2) e^{-t^2/2} \tag{7}$$

The Fourier transform of the Mexican hat function has maxima at $f = \pm \sqrt{2}/(2\pi)$, which provide convenient characteristic frequencies for the wavelet. Thus, to facilitate comparison with Fourier methods, we chose to associate the wavelet scale with a nondimensional frequency

$$f_a = \sqrt{2}/(2\pi a) \tag{8}$$

This characteristic frequency should be comparable to the frequency in the Fourier transform to within an order of magnitude.

An alternative wavelet function is given by the negative of the first derivative of the Gaussian function. This wavelet is useful for detecting sharp changes in value in a signal (see Figs. 2c and 2d), and we call it the slope detector wavelet. It has the following form:

$$g(t) = t e^{-t^2/2} \tag{9}$$

The Fourier transform of Eq. (9) has maxima at $f = \pm 1/(2\pi)$, and thus we chose the characteristic frequency as

$$f_a = 1/(2\pi a) \tag{10}$$

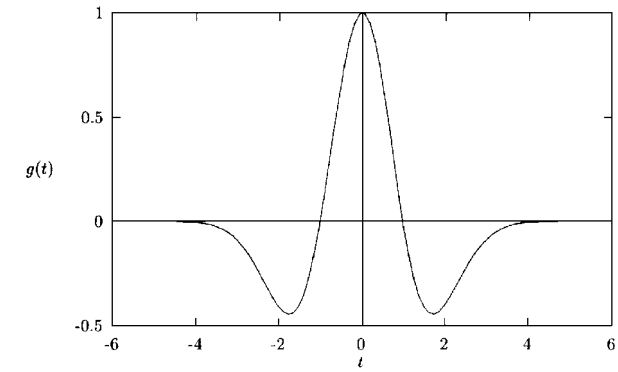


**a) Mexican hat function in time domain**

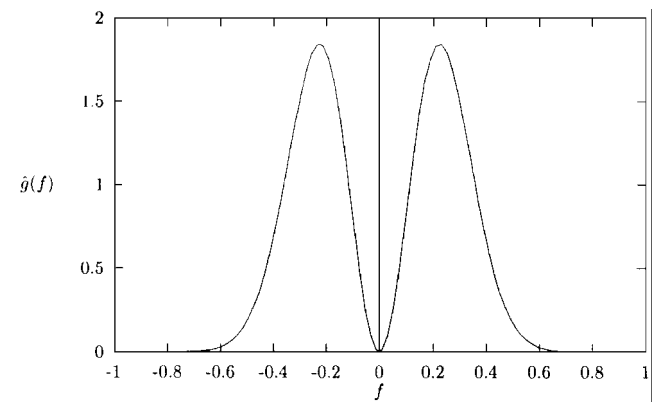


**b) Mexican hat function in frequency domain**

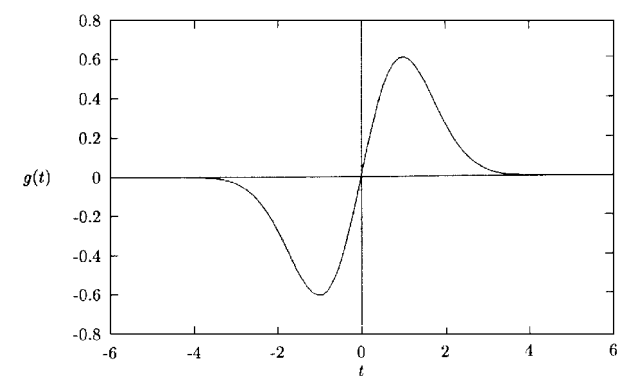


**c) Slope detector function in time domain**

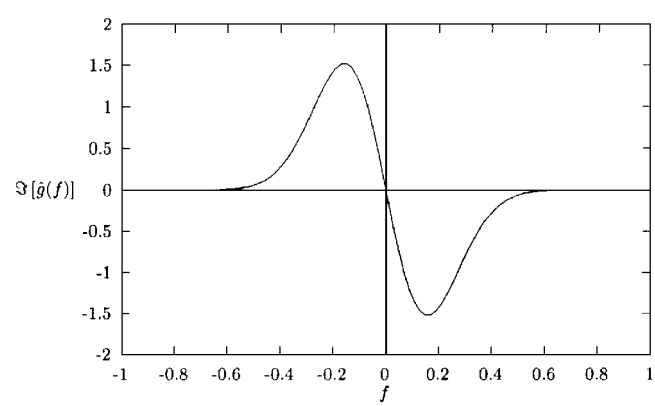


**d) Slope detector function in frequency domain**

**Fig. 2 Wavelet functions.**

It can be shown that the reconstruction parameter $C_\psi = \pi$ for both wavelets. Further, both meet the requirements of zero mean and finite energy.

The data were analyzed with a software package developed by the authors. The signal level was normalized by the local mean and standard deviation, whereas time, frequency, and wavelet scale were nondimensionalized by the characteristic time $\theta / U_e$.

For computational efficiency, the convolution integrals of Eqs. (1) and (3) were implemented by using a fast Fourier transform algorithm (e.g., Ref. 33). The wavelet scale was discretized according to a power law $a \propto a_0^m$, and the integration over the wavelet scales was performed by using the trapezoidal rule.

## Results

Figure 3 shows the distribution of the intensity of the wall-pressure fluctuations (as measured by the standard deviation of the pressure signal) along the wind-tunnel centerline upstream of the fin. Data obtained by Dolling and Bogdonoff[12] at the same Mach number are shown for comparison; there is generally good agreement even though $D/\delta = 0.80$ for their study and $D/\delta = 0.68$ for this work. The random motion of the separation shock is evident as a peak in the intensity of the pressure fluctuations at $x/D \approx -2.5$, whereas the local maximum at $x/D \approx -1.0$ may be associated with reattachment unsteadiness or possibly a second separation shock.

We focus on the pressure fluctuation data obtained at two stations in the region of separation shock unsteadiness: $x/D = -2.93$ and $-2.67$. A pair of simultaneous segments of the signals from the two transducers are shown in Fig. 4. In each plot, the signal level is normalized by the local mean and standard deviation, and the time is nondimensionalized by the characteristic time scale $\theta / U_e$.

The data display the intermittent character often found in wall-pressure measurements obtained in separated supersonic flows. Kistler,[34] in a study of a forward-facing step flow, was probably the first to observe this pattern and to identify the two components of the signal with changes in the geometry of the separated region and with turbulent fluctuations. When the separation shock is located relatively far downstream or upstream from a given pressure transducer, the pressure fluctuations are, respectively, representative of the turbulence in the incoming boundary layer or in the fin root vortex flow. When the separation shock passes over the transducer, however, there is a sharp change in the pressure level: an increase if the shock moves upstream of the transducer and a decrease if the shock passes downstream of the transducer. The result is a series of pulses of random duration in the pressure signal.

For the upstream station (Fig. 4a), the shock is typically located downstream of the transducer, but it makes occasional excursions upstream. In contrast, the signal from the downstream station (Fig. 4b) is highly intermittent because of frequent shock-crossing events. The correlation between the pair of signals is clear; close inspection of the plots reveals downstream convection of small-scale features in the signals as well as synchronized shock-crossing events.

Our aim in this work is to extract the characteristic time scales of the shock motion and of the flow turbulence from the wall-pressure signals. We first examine how the total signal energy is distributed over different frequencies in the Fourier energy spectrum. The spectra were calculated by the procedures of Bendat and Piersol.[33] Windows of 1024 points, with 50% overlap, were tapered with the Hanning window, processed using a fast Fourier transform algorithm, and averaged.

The Fourier spectra for the two stations under consideration are shown in Fig. 5. The data are normalized by the local standard

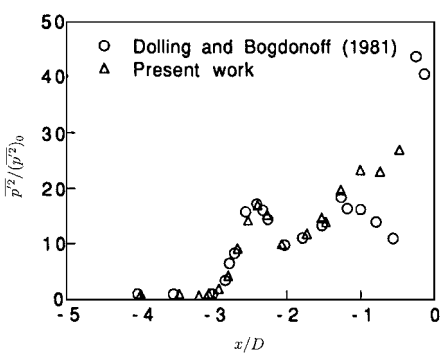


**Fig. 3 Intensity of wall-pressure fluctuations on the wind-tunnel centerline upstream of the fin ($y = z = 0$). Data of Dolling and Bogdonoff[12] are plotted for comparison.**

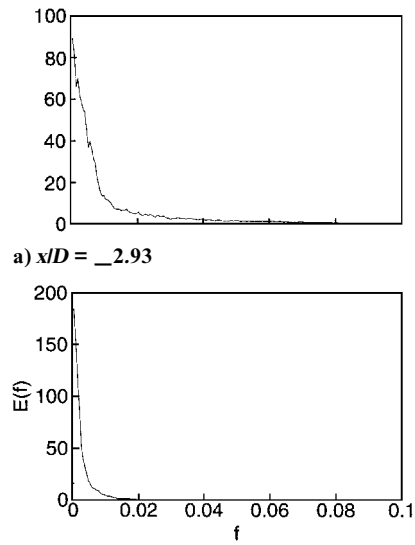


**a) $x/D = -2.93$**

**b) $x/D = -2.67$**

**Fig. 5 Fourier energy spectra.**

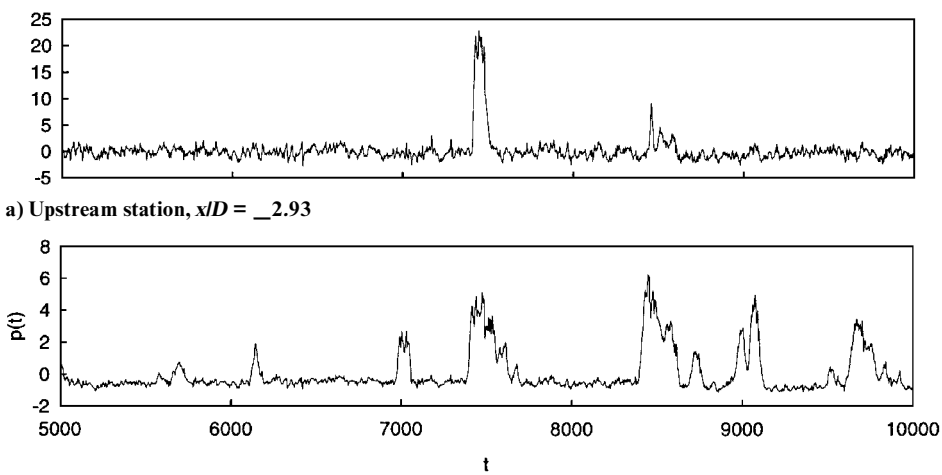


**a) Upstream station, $x/D = -2.93$**

**b) Downstream station, $x/D = -2.67$**

**Fig. 4 Time series plots.**

deviation of the signal level and the time scale $\theta/U_e$. We have chosen to display the spectra on linear axes to illustrate how the Fourier transform assigns most signal energy to low frequencies (large time scales). The effect of the frequent shock-crossing events in the case of $x/D = -2.67$ measurement is shown in the power spectrum as an additional shift in energy content into the low-frequency range.

We wish to compare the distribution of energy under the Fourier transform to the way the wavelet transform assigns energy to different time scales. The wavelet energy spectrum, defined by Eq. (6), is shown for the two channels of data in Fig. 6, where solid lines correspond to the spectrum for the Mexican hat wavelet and dot-dashed lines represent the spectrum for the slope detector wavelet.

As with the Fourier spectrum, the wavelet spectrum assigns most of the signal energy to large scales and low frequencies. (Note the long tails for large wavelet scale.) However, the wavelet spectrum displays distinct maxima that are not found in the Fourier spectrum. We label the scales corresponding to the maxima $a_B$ and $a_S$ for boundary layer and shock, respectively, and call the corresponding frequencies $f_B$ and $f_S$. For the data taken at the upstream station ($x/D = -2.93$), the wavelet spectrum shows a maximum at small scale (around $a_B = 2$ or $f_B = 0.1$) and gradually falls off for larger time scales. The data from the downstream station ($x/D = -2.67$) have a relative maximum at this small scale but also show a peak at larger scale. For the Mexican hat wavelet, this local maximum occurs at about $a_S = 26$ or $f_S = 0.9 \times 10^{-2}$; for the slope detector wavelet, it occurs around $a_S = 14$ or $f_S = 1.2 \times 10^{-2}$. The width of the wavelet functions (see Fig. 2) at this scale is about $8a_S \approx 10^2$, consistent with the width of the pulses in the time series plots of Fig. 4.

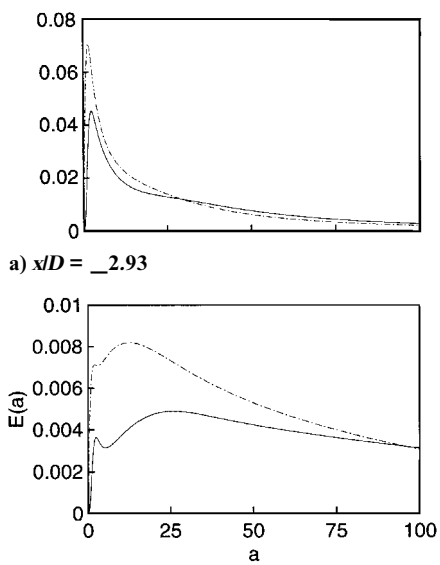


a) $x/D = -2.93$

b) $x/D = -2.67$

**Fig. 6 Wavelet energy spectra.**

The two maxima observed in the wavelet energy spectrum motivate filtering in the wavelet domain to separate the two components of the wall-pressure signal. Filtering can be accomplished by applying the reconstruction formula [Eq. (3)] over a restricted range of scales.

First we consider a reconstruction with all the available wavelet scales. Figure 7a shows a sample of the results. For this case, the original signal (Fig. 4b) displays the characteristic pulses associated with shock-crossing events as well as the small-scale fluctuations associated with turbulent flow upstream and downstream of the shock wave. The reconstructed signal captures these features well, although the limited range of wavelet scales available for reconstruction introduces some drift in the baseline pressure level and a smoothing of the smallest scales.

We would like to split the signal into two parts, one associated with the characteristic time scale of the shock-crossing events and the other associated with the relatively smaller scale turbulent fluctuations. It would be satisfying if a simple cutoff at the minimum in the wavelet spectrum would split the components cleanly, but because of the overlap in energy content between the two signal components the most effective separation was obtained by splitting the signal at the scale $a_S$ associated with the shock motion.

Figures 7b and 7c illustrate the results of filtering. A sample of the reconstruction by using the low-frequency ($f_{\min} < f < f_S$), large-scale ($a_S < a < a_{\max}$) portion of the spectrum is shown in Fig. 7b. The small-scale turbulent fluctuations have been quite effectively removed by this filtering; only the pattern associated with the shock-crossing events remains.

This filtering could be quite useful for conditioning a signal before applying a threshold to discriminate between a shock-upstream and a shock-downstream condition. Liandrat and Moret-Bailly[35] used such a method to examine an oblique shock perturbed by freestream turbulence, but they chose an arbitrary cutoff scale for filtering the

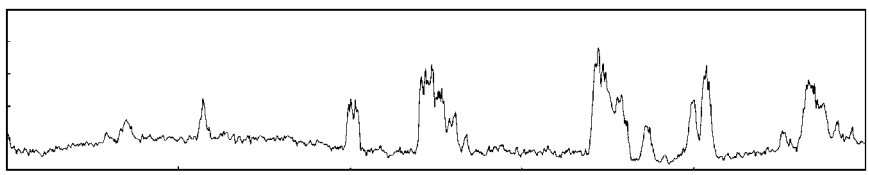

a) Signal reconstructed with all available scales

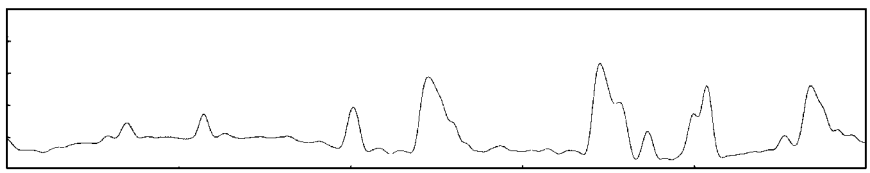

b) Low-pass filter ( $f_{\min} < f < f_S$, $a_S < a < a_{\max}$)

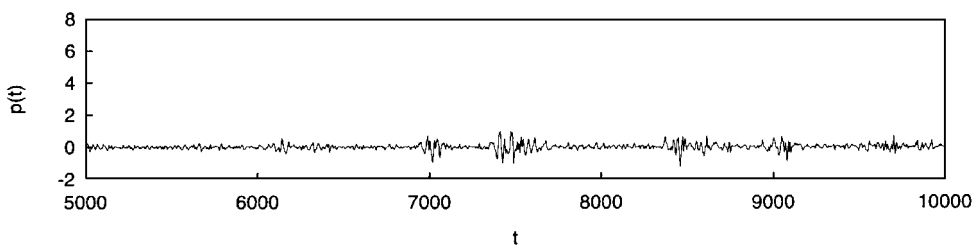


c) High-pass filter ( $f_S < f < f_{\max}$, $a_{\min} < a < a_S$)

**Fig. 7 Inverse transform with Mexican hat wavelet for $x/D = -2.67$.**

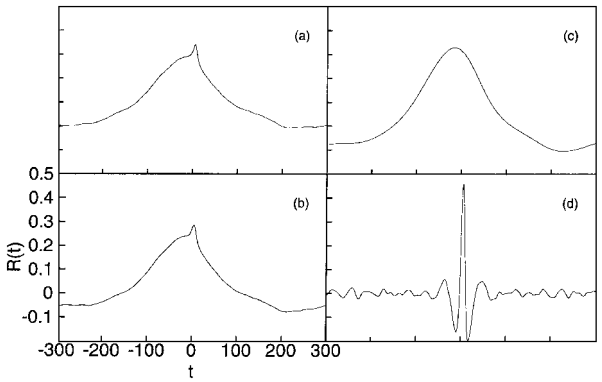


**Fig. 8 Cross correlation between signals from $x/D = -2.93$ and $-2.67$: a) original signal, b) signal reconstructed with all available scales, c) low-pass filter ($a_S < a < a_{max}$), and d) high-pass filter ($a_{min} < a < a_S$).**

signal. The current results show that extrema in the wavelet energy spectrum provide characteristic time scales of the flow, which can be used for physically meaningful filtering of the signal.

The corresponding high-frequency ($f_S < f < f_{max}$), small-scale ($a_{min} < a < a_S$) reconstruction is shown in Fig. 7c. Interestingly, this signal contains regions of high amplitude associated with periods in which the shock is upstream of the transducer. These regions appear to reflect the higher-amplitude fluctuations present in the flow downstream of the shock wave.

A quantitative assessment of the effectiveness of the filtering in splitting the two components of the signal can be obtained through cross-correlations. The cross-correlations were performed by a fast Fourier transform procedure,[33] with windows of 1024 points augmented with an equal segment of zero padding. The cross-correlation of the raw signals is shown in Fig. 8a (see also Ref. 4). The characteristic overall width of the correlation ($t$ of a few hundred) corresponds closely to the characteristic width of the shock-crossing pulses in the time-series plots. An interesting narrow peak is evident at positive time delay; the corresponding convection velocity of about $0.75U_e$ corresponds nicely to the turbulent boundary layer results of Spina and Smits[29] for the same Mach number. The cross correlation of the reconstructed signals (Fig. 8b) mimics the shape of the correlation of the raw signals but appears shifted down. This effect seems to be due to neglected large-scale information.

Cross correlations corresponding to the wavelet-filtered time-series data of Fig. 7 are shown in Figs. 8c and 8d. As expected from the appearance of the time-series plots, the cross correlation of the low-pass-filtered signals (Fig. 8c) shows no evidence of the small-scale component of the signal; it reflects only the large-scale shock-crossing phenomenon. The correlation of the high-pass-filtered signals (Fig. 8d) shows the complementary phenomenon: a sharp peak at the time delay corresponding to the boundary-layer convection velocity.

We note that the two possible correlations between a high-pass-filtered signal and a low-pass-filtered signal (not shown) are extremely low: less than 0.02. There seems to be a weak connection between the phenomena occurring at the two signal time scales.

## Concluding Remarks

The wavelet transform offers a fresh approach to the problem of inferring flow structure from measurements of wall-pressure fluctuations in flows with shock oscillation. Past approaches to this problem have indirectly identified the time scales in the wall-pressure signal associated with large-scale turbulence structures and shock-crossing events. The wavelet transform directly identifies these time scales as distinct maxima in the wavelet energy spectrum, and the scales can serve as a reference for filtering in the space of wavelet scales.

A basic question of engineering interest about the separation shock oscillation problem is how the characteristic intensity and frequency of the wall-pressure fluctuations correlate with the flow boundary conditions. The wavelet transform provides a tool for characterizing the pressure signal, and application of the wavelet transform may lead to improved correlations of the relevant parameters.

To attack the problem of the cause of the shock unsteadiness, we need to correlate the time history of the position of the separation shock with parameters characterizing the time evolution of large-scale structures in the incoming turbulent boundary layer and the vortex shedding cycle in the separated region at the fin root. An approach that combines wall-pressure measurements with simultaneous flow visualization seems quite promising. The wavelet transform can contribute here by separating the footprint of the shock motion from the contribution of turbulent pressure fluctuations.

## Acknowledgments

This study was carried out as part of a research program supported by NASA Lewis Research Center Grant NAG3-1022, monitored by W. Hingst. Additional support was provided by Air Force Office of Scientific Research URI Grant 90-0217. J. Poggie received support under the U.S. Air Force Senior Knight Employment Program. The experimental data analyzed in this paper were obtained by T. Evans and K. Poddar. K. Poddar carried out a preliminary analysis of the data with the wavelet transform. The software used in the wavelet analysis was developed in collaboration with R. Smith. J. Poggie would like to acknowledge valuable discussions of this work with R. Kimmel and A. Creese.

## References

[1]Thomas, A. S. W., "The Unsteady Characteristics of Laminar Juncture Flow," *Physics of Fluids*, Vol. 30, No. 2, 1987, pp. 283–285.

[2]Visbal, M. R., "Structure of Laminar Juncture Flows," *AIAA Journal*, Vol. 29, No. 8, 1991, pp. 1273–1282.

[3]Erengil, M. E., and Dolling, D. S., "Physical Causes of Separation Shock Unsteadiness in Shock Wave/Turbulent Boundary Layer Interactions," AIAA Paper 93-3134, July 1993.

[4]Brusniak, L., and Dolling, D. S., "Physics of Unsteady Blunt-Fin-Induced Shock Wave/Turbulent Boundary Layer Interactions," *Journal of Fluid Mechanics*, Vol. 273, 1994, pp. 375–409.

[5]Forkey, J., Cogne, S., Smits, A., and Bogdonoff, S., "Time-Sequenced and Spectrally-Filtered Rayleigh Imaging of Shock Wave and Boundary Layer Structure for Inlet Characterization," AIAA Paper 93-2300, June 1993.

[6]Poggie, J., "On the Control of a Compressible, Reattaching Shear Layer," Ph.D. Dissertation, Dept. of Mechanical and Aerospace Engineering, Princeton Univ., Princeton, NJ, 1995.

[7]Bogar, T. J., "Structure of Self-Excited Oscillations in Transonic Diffuser Flows," *AIAA Journal*, Vol. 24, No. 1, 1986, pp. 54–61.

[8]Kussoy, M. I., Brown, J. D., Brown, J. L., Lockman, W. K., and Horstman, C. C., "Fluctuations and Massive Separation in Three-Dimensional Shock-Wave/Boundary-Layer Interactions," *Transport Phenomena in Turbulent Flows: Theory, Experiment, and Numerical Simulation*, edited by M. Hirata and N. Kasagi, Hemisphere, New York, 1988, pp. 875–887.

[9]Dolling, D. S., and Brusniak, L., "Correlation of Separation Shock Motion in a Cylinder-Induced Interaction with Pressure Fluctuations Under the Separated Region," AIAA Paper 91-0650, Jan. 1991.

[10]Eaton, J. K., and Johnston, J. P., "Low Frequency Unsteadiness of a Reattaching Turbulent Shear Layer," *Turbulent Shear Flows 3*, edited by L. J. S. Bradbury, F. Durst, B. E. Launder, F. W. Schmidt, and J. H. Whitelaw, Springer, Berlin, 1982, pp. 162–170.

[11]Loth, E., and Matthys, M. W., "Unsteady Low Reynolds Number Shock Boundary Layer Interactions," *Physics of Fluids*, Vol. 7, No. 5, 1995, pp. 1142–1150.

[12]Dolling, D. S., and Bogdonoff, S. M., "An Experimental Investigation of the Unsteady Behavior of Blunt Fin-Induced Shock Wave Turbulent Boundary Layer Interactions," AIAA Paper 81-1287, June 1981.

[13]Aso, S., Hayashi, M., and Tan, A., "The Structure of Aerodynamic Heating in Three-Dimensional Shock Wave/Turbulent Boundary Layer Interactions Induced by Sharp and Blunt Fins," AIAA Paper 89-1854, June 1989.

[14]Shifen, W., and Qingquan, L., "Hypersonic Turbulent Separated Flow Past an Unswept Circular Cylinder on a Flat Plate," *Acta Aerodynamica Sinica*, Vol. 10, No. 1, 1992, pp. 38–44.

[15]Hung, C.-M., and Buning, P. G., "Simulation of Blunt-Fin-Induced Shock-Wave and Turbulent Boundary-Layer Interaction," *Journal of Fluid Mechanics*, Vol. 154, 1985, pp. 163–185.

[16]Lakshmanan, B., and Tiwari, S. N., "Study of Supersonic Intersection Flowfield at Modified Wing-Body Junctions," *AIAA Journal*, Vol. 31, No. 5, 1993, pp. 877–883.

[17]Sedney, R., and Kitchens, C. W., "Separation Ahead of Protuberances in Supersonic Turbulent Boundary Layers," *AIAA Journal*, Vol. 15, No. 4, 1977, pp. 546–552.

[18]Dolling, D. S., and Bogdonoff, S. M., "Scaling of Interactions of Cylinders with Supersonic Turbulent Boundary Layers," *AIAA Journal*, Vol. 19, No. 5, 1981, pp. 655–657.

[19]Dolling, D. S., and Bogdonoff, S. M., "Blunt Fin-Induced Shock Wave/Turbulent Boundary-Layer Interaction," *AIAA Journal*, Vol. 20, No. 12, 1982, pp. 1674–1680.

[20]Dolling, D. S., Cosad, C. D., and Bogdonoff, S. M., "An Examination of Blunt-Fin Induced Shock Wave Turbulent Boundary Layer Interactions," AIAA Paper 79-0068, Jan. 1979.

[21]Smith, D. R., Poggie, J., Konrad, W., and Smits, A. J., "Visualization of the Structure of Shock Wave Turbulent Boundary Layer Interactions Using Rayleigh Scattering," AIAA Paper 91-0651, Jan. 1991.

[22]Gramann, R. A., and Dolling, D. S., "Detection of Turbulent Boundary Layer Separation Using Fluctuating Wall Pressure Signals," *AIAA Journal*, Vol. 28, No. 6, 1990, pp. 1052–1056.

[23]Kaufman, L. G., Korkegi, R. H., and Morton, L. C., "Shock Impingement Caused by Boundary Layer Separation Ahead of Blunt Fins," *AIAA Journal*, Vol. 11, No. 10, 1973, pp. 1363–1364.

[24]Gramann, R. A., and Dolling, D. S., "Interpretation of Separation Lines from Surface Tracers in a Shock-Induced Turbulent Flow," *AIAA Journal*, Vol. 25, No. 12, 1987, pp. 1545, 1546.

[25]Gonsalez, J. C., and Dolling, D. S., "Correlation of Interaction Sweepback Effects on the Dynamics of Shock-Induced Turbulent Separation," AIAA Paper 93-0776, Jan. 1993.

[26]Evans, T., Poddar, K., and Smits, A. J., "Compilation of Wall Pressure Data for a Shock Wave Boundary Layer Interaction Generated by a Blunt Fin," Dept. of Mechanical and Aerospace Engineering, Princeton Univ., Princeton, NJ, Dec. 1990.

[27]Poggie, J., Poddar, K., and Smits, A. J., "Application of the Wavelet Transform to the Study of Unsteady Pressure Loading in a Blunt-Fin-Induced Shock Wave/Boundary Layer Interaction," *Forum on Unsteady Flows*, edited by W. L. Keith and T. Wei, Vol. 157, Fluids Engineering Div., American Society of Mechanical Engineers, New York, 1993, pp. 57–72.

[28]Settles, G. S., "An Experimental Study of Compressible Turbulent Boundary Layer Separation at High Reynolds Number," Ph.D. Dissertation, Dept. of Mechanical and Aerospace Engineering, Princeton Univ., Princeton, NJ, 1975.

[29]Spina, E. F., and Smits, A. J., "Organized Structures in a Compressible Turbulent Boundary Layer," *Journal of Fluid Mechanics*, Vol. 182, 1987, pp. 85–109.

[30]Dolling, D. S., and Dussauge, J. P., "Fluctuating Wall-Pressure Measurements," *A Survey of Measurements and Measuring Techniques in Rapidly Distorted Compressible Turbulent Boundary Layers*, edited by E. Reshotko, AGARDograph No. 315, 1989, pp. 8-1–8-18.

[31]Vetterli, M., and Kovačevíc, J., *Wavelets and Subband Coding*, Signal Processing Series, Prentice–Hall, Englewood Cliffs, NJ, 1995.

[32]Farge, M., "Wavelet Transforms and Their Applications to Turbulence," *Annual Review of Fluid Mechanics*, Vol. 24, 1992, pp. 395–457.

[33]Bendat, J. S., and Piersol, A. G., *Random Data: Analysis and Measurement Procedures*, 2nd ed., Wiley, New York, 1986.

[34]Kistler, A. L., "Fluctuating Wall Pressure under a Separated Supersonic Flow," *Journal of the Acoustical Society of America*, Vol. 36, No. 3, 1964, pp. 543–550.

[35]Liandrat, J., and Moret-Bailly, F., "The Wavelet Transform: Some Applications to Fluid Dynamics and Turbulence," *European Journal of Mechanics B/Fluids*, Vol. 9, No. 1, 1990, pp. 1–19.

R. W. Wlezien
*Associate Editor*